RSC Advances

PAPER

View Article Online
View Journal | View Issue

Cite this: *RSC Adv.*, 2025, **15**, 14042

Silk-based microparticles for the adsorption of methylene blue: formulations, characterization, adsorption study, *in silico* molecular docking, and molecular dynamics simulation†

Duy Toan Pham,[a] Phuong T. M. Ha,[b] Ngoc Bich Pham,[a] Ngoc Yen Nguyen,[a] Ngoc Thanh Vo,[a] Dang Khoa Dang,[c] Danh Si Ra,[d] Anh Minh Pham-Phan,[e] Manh Quan Nguyen[f] and Bui Thi Phuong Thuy *[g]

Although silk-derived biomaterials have garnered attention for environmental remediation due to their sustainability, biocompatibility, and biodegradability, the application of silk fibroin-based microparticles (FNP) for pollutant dye adsorption remains vastly underexplored. Hence, this study pioneers the fabrication and characterization of FNP for the removal of methylene blue (MB), offering a comprehensive comparison with two other silk-based states of raw silk cocoon pieces (SC) and sericin-degummed silk fibers (SD). Remarkably, FNP achieved an adsorption capacity of 122.98 mg g^{-1}, over 32-fold higher than both SC and SD (3.8 mg g^{-1}), highlighting its superior efficiency. The adsorption performance of FNP was strongly influenced by experimental variables including pH, contact time, initial dye concentration, and adsorbent dosage. Structurally, FNP exhibited favorable physicochemical properties for adsorption, including uniform spherical morphology (~2.45 μm), moderate surface area (21.894 m^2 g^{-1}), a mesoporous-to-macroporous structure (pore diameter 21.911 Å), and a point of zero charge (pH_{pzc}) of 6.7, contributing to its effective electrostatic interactions with the cationic dye MB. Importantly, the adsorption data fitted the Dubinin–Radushkevich isotherm, indicating a chemisorption-dominated mechanism. Molecular docking further revealed specific fibroin-dye interactions at Lys62 (hydrogen bonding, −0.2 kcal mol^{-1}) and Glu94 (ionic bonding, −1.9 kcal mol^{-1}). Additionally, molecular dynamics simulations in water confirmed the docking results and demonstrated the aqueous stability of the fibroin-MB complex. Conclusively, this work not only establishes FNP as a high-performance, eco-friendly adsorbent for MB removal, but also provides mechanistic insights at the molecular level, offering a scientific foundation for the rational design of protein-based adsorbents in future environmental technologies.

Received 1st April 2025
Accepted 24th April 2025

DOI: 10.1039/d5ra02266e

rsc.li/rsc-advances

1. Introduction

Methylene blue (MB), a green organic dye from the phenothiazine family with several uses in medicine and textile dyeing, dissociates as cations (MB^+).[1] MB serves as a prime example of an environmental threat. Toxic gases created during MB decomposition include Cl_2, NO_2, CO, SO_2, CO_2, and H_2S. Discharging MB into the aquatic environment decreases light penetration and causes poisons to enter the food chain of creatures.[2] MB exhibits a high molar absorption coefficient (~8.4×10^4 L mol^{-1} cm at 664 nm), which reduces sunlight penetration, thereby impairing photosynthetic activity and oxygen solubility in aquatic environments.[3] Even at low concentrations, MB can generate intensely colored byproducts that disrupt aquatic biodiversity and ecosystem aesthetics. Furthermore, MB is non-biodegradable, carcinogenic, and hazardous to human health, potentially causing respiratory failure, vision impairment, digestive disorders, and neurological issues.[4] Therefore, addressing these environmental and health concerns necessitates innovative approaches for the effective adsorption and removal of MB.

Currently, several materials and advanced methods/technologies have been employed for the removal of harmful

[a]Department of Health Sciences, College of Natural Sciences, Can Tho University, Can Tho, Vietnam
[b]Department of Chemistry, Faculty of Pharmacy and Nursing, Tay Do University, 68 Tran Chien Street, Can Tho, Vietnam
[c]Lac Hong University, No. 10 Huynh Van Nghe Str., Buu Long Ward, Bien Hoa, Dong Nai, Vietnam
[d]Dam Ca Mau Factory – Petrovietnam Camau Fertilizer Joint Stock Company (PVCFC), Ca Mau, Vietnam
[e]DHG Pharmaceutical Joint-Stock Company, Can Tho, Vietnam
[f]Department of Analytical Chemistry-Drug Quality Control, Faculty of Pharmacy, Can Tho University of Medicine and Pharmacy, Can Tho, Vietnam
[g]Faculty of Fundamental Sciences, Van Lang University, Ho Chi Minh City, Vietnam. E-mail: thuy.btp@vlu.edu.vn

† Electronic supplementary information (ESI) available. See DOI: https://doi.org/10.1039/d5ra02266e

substances and ions from aqueous solutions and environments.[5–7] For that reason, MB is similarly adsorbed and treated using these technologies and materials. Previous studies have explored the use of natural and synthetic materials for the adsorption of MB. Activated carbon, derived from various biomass sources, has been widely investigated due to its high porosity and surface area, but its high production cost limits scalability.[8] Similarly, nanocellulose and nanolignin have been studied for their effectiveness in MB adsorption; these materials exhibit high adsorption properties but face challenges related to large-scale synthesis and application.[9] To address these limitations, a novel potential material is necessary for the adsorption of MB.

Silkworm cocoons, a primary raw material in textile production, hold untapped potential for addressing this issue.[10] Silk cocoons are made up of a matrix of continuous silk threads that are roughly 1000–1500 meters long and bound together with sericin.[11] As a result, silk cocoon pieces have a huge specific surface area and excellent adsorption capabilities. Furthermore, silk fibroin, the structural protein in silk, offers unique advantages for MB adsorption due to its ability to self-assemble into nanoparticles. Previous studies have demonstrated the effectiveness of silk fibroin in MB adsorption when used in forms like regenerated silk fibroin membranes and hydrogels, owing to their porosity and strong interactions with cationic dyes.[12–16] For instance, silk fibroin membranes modified with functional groups were shown to achieve high adsorption capacities due to enhanced electrostatic interactions with MB molecules.[12] Moreover, the silk fibers have also been used as an effective MB adsorption material.[17]

Despite these advancements, research on fibroin nanoparticles (FNP) for MB adsorption remains limited. FNP possess a negatively charged surface, high specific surface area, and a matrix-like structure that facilitates electrostatic interactions with cationic dyes such as MB.[18] These characteristics make FNP a novel and highly effective material for MB adsorption. Moreover, FNP can be derived from waste materials such as silk cocoon pieces, aligning with the principles of waste valorization and sustainability. This novel approach not only addresses the environmental challenge of MB removal but also presents an efficient, scalable, and eco-friendly solution. Additionally, the in-depth fibroin-MB interaction mechanisms are lacking.

Herein, this study aims to evaluate and compare the MB adsorption performance of silk cocoon pieces (SC), sericin-degummed silk strands (SD), and FNP. Moreover, in-depth analysis on the MB and fibroin interactions are also investigated using *in silico* docking and molecular dynamics simulation study.

2. Methods and materials

2.1 Materials

Raw silk cocoons (SC) were sourced from Nam Dinh, Vietnam. Chemicals including sodium carbonate (Na_2CO_3, ≥99.5%), calcium chloride ($CaCl_2$, ≥96.0%), ethanol (EtOH, ≥99.7%), and calcium nitrate tetrahydrate ($Ca(NO_3)_2 \cdot 4H_2O$, ≥99.0%) were procured from Xilong Chemical Co. MB (dye content ≥82%) was obtained from Sigma-Aldrich, ensuring high purity for experimental accuracy. All chemicals were used as received without further purification.

2.2 Preparation of adsorbents

In this study, three adsorbents were employed, demonstrating three distinct forms of fibroin, including the SC, the sericin-degummed silk strands (SD), and the FNP. The SC was used as obtained. The SD were fabricated by dissolving the SC in 0.5% (w/v) Na_2CO_3 at 100 °C for 1 h, followed by washing thrice with water and air-drying.[19] Both SC and SD were cut into 0.1 mm pieces to increase the surface area for adsorption.

The FNP were synthesized through a solvent exchange method.[20] Briefly, the previously obtained SD was dissolved at a temperature of 90 °C for approximately 10 min in a mixture of $CaCl_2$, $Ca(NO_3)_2$, water, and ethanol, combined in a ratio of 30 : 5 : 45 : 20 (w/w/w/w). This mixture was made by dissolving the pure $CaCl_2$ and $Ca(NO_3)_2$ powders in water, followed by the addition of ethanol at the aforementioned ratio. The resulting fibroin solution, after being dissolved in calcium mixture, was then dialyzed against water at room temperature (25 °C) for 4 days using a cellulose membrane with a molecular weight cut-off of 10 000. The concentration of the silk fibroin solution was determined using UV-vis spectroscopy at a wavelength of 276 nm. A standard curve was created within the concentration range of 0.1–1 mg mL^{-1}, applying the linear regression equation $y = 1.1517x + 0.0099$ with an R^2 value of 0.9999 to quantify the fibroin content. Then, the prepared fibroin solution (1% w/v) was added dropwise into 5 mL of absolute ethanol under constant agitation at 150 rpm for 15 min. The resulting mixture was centrifuged (12 000 rpm, 30 min) to separate the FNP, which were washed with water to remove any residual ethanol. The FNP were freeze-dried (−55 °C, 200 mTorr, 48 h) and kept at 4 °C until uses. This process was selected for its simplicity and high scalability, making it well-suited for subsequent in-production investigations.

2.3 MB adsorption study

The adsorption performance of SC, SD, and FNP was evaluated by dispersing each material in 20 mL of MB solution at initial concentrations of 5, 10, 20, 30, and 40 μg mL^{-1}. The mixtures were agitated at 150 rpm for 30 min to assess the effect of MB concentration on adsorption capacity. The adsorption equilibrium data obtained were used to develop isotherm models.

To evaluate the influence of adsorbent mass, varying amounts of SC and SD (0.1, 0.2, 0.4, 0.6, and 0.8 g) and FNP (0.003, 0.006, 0.012, 0.024, and 0.036 g, corresponding to nanoparticles derived from 0.5, 1, 2, 3, 4, and 5 mL of 1% fibroin solution, respectively) were tested under similar experimental conditions. Similarly, the effect of contact time was examined by maintaining a constant MB concentration and adsorbent mass while varying the agitation duration (15, 30, 45, 60, 90, and 120 min). Finally, to establish the optimal adsorption environment, the influence of pH on adsorption efficiency was studied by adjusting the MB solution's pH to 2, 4, 6, and 8 using 0.1 M NaOH or 0.1 M HCl. All experiments were conducted under similar conditions to ensure comparability. The full list of these variables is presented in Table 1.

The residual MB concentration after the adsorption process was calculated using the standard curve $y = 0.3816x - 0.044$, R^2

Table 1 Absorption study variables and their investigated values ranges

Variable	Investigated values
MB initial concentration	5, 10, 20, 30, and 40 μg mL^{-1}
Adsorbent mass (SC, SD)	0.1, 0.2, 0.4, 0.6, and 0.8 g
Adsorbent mass (FNP)	0.003, 0.006, 0.012, 0.024, and 0.036 g
Adsorption time	15, 30, 45, 60, 90, and 120 min
pH	2, 4, 6, and 8

= 0.9990, and a maximum wavelength of 662 nm. The adsorption efficiency was calculated by formula (1), where C_0 and C_e are the initial and equilibrium MB concentrations (mg L^{-1}), respectively.

$$\%H = \frac{(C_0 - C_e)}{C_0} \times 100(\%) \quad (1)$$

Adsorption equilibrium and kinetic models were developed using the following equations.[21–23]

$$\text{Langmuir isotherm}: \frac{C_e}{q_e} = \frac{1 \times C_e}{q_m} + \frac{1}{q_m \times K_L}$$

$$\text{Freundlich isotherm}: \log q_e = \log K_F + \frac{1}{n} \times \log C_e$$

$$\text{Dubinin} - \text{Radushkevich(D} - \text{R)}:$$

$$\ln q_e = \ln q_m - \beta\varepsilon^2; \varepsilon = RT \ln\left(1 + \frac{1}{C_e}\right); E = \frac{1}{\sqrt{2\beta}}$$

$$\text{Pseudo-first-order kinetics: } \ln(q_e - q_t) = \ln(q_e) - k_1 t$$

$$\text{Pseudo-second-order kinetics}: \frac{t}{q_t} = \frac{1}{k_2 q_e^2} + \frac{t}{q_e}$$

where k_1 (min^{-1}) and k_2 (g mg^{-1} min^{-1}) are the rate constants for pseudo-first-order and pseudo-second-order kinetics, respectively; q_e (mg g^{-1}) and q_t (mg g^{-1}) represent the equilibrium and time-dependent adsorption capacities; t is the contact time (min); C_e and C_0 are the equilibrium and initial MB concentrations (mg L^{-1}); q_m (mg g^{-1}) is the maximum adsorption capacity; K_L and K_F are the Langmuir and Freundlich constants, respectively; $1/n$ describes adsorption intensity; β (mol^2 J^{-2}) relates to mean adsorption energy; ε is the Polanyi potential; and E (kJ mol^{-1}) represents the mean free energy of adsorption.

To further evaluate the FNP regeneration/reusability, multiple adsorption–desorption cycles were performed. For this, after the FNP were used to adsorbed MB under the optimal condition, the FNP-MB was being centrifuged to separate the particles and subjected to a desorption process to remove the adsorbed MB. Then, the FNP were washed, dried, and reused in a subsequent adsorption cycle. This cycle was repeated three times, and the adsorption efficiency was measured after each cycle.

2.4 Physicochemical characterizations

The adsorbents were physicochemically characterized, where appropriate, the following parameters.

2.4.1 Adsorbent total nitrogen content. The total nitrogen content of the adsorbent (*i.e.*, SC, SD, and FNP) was measured using the standard Dumas combustion method. This method works by completely oxidizing a sample at high temperatures, converting all nitrogen-containing compounds into nitrogen gas, which is then measured to determine the nitrogen content utilizing a thermal conductivity detector. Briefly, a sample mass of approximately 0.1 g was weighed, subjected to the analysis instrument (FP928 Nitrogen and Protein Analyzer, Leco, USA), Dam Ca Mau Factory – Petrovietnam Camau Fertilizer Joint Stock Company (PVCFC), and run using the standard settings incorporated in the machine.

2.4.2 Adsorbent size. For the SC and SD, the average sizes were determined based on the SEM micrographs (described in the next section).

For the FNP, the average size of the particles and size distribution (polydispersity index, PI) were assessed using a MicroTrac S3500 analyzer by dynamic light scattering (DLS). Briefly, the FNP were re-dispersed in water to a count rate of 500–600 kcps. Then, the dispersions were put into a polystyrene cuvette, followed by standard measurements as instructed by the machine manufacturer.

2.4.3 Adsorbent morphology. The adsorbent morphology was assessed using the scanning electron microscopy (SEM) analysis, by the Carl Zeiss instrument. The samples were immobilized on a carbon-coated disc mounted on a metal substrate, followed by spin-coated with a 10 nm layer of gold. Then, the samples were observed using SEM, under a nitrogenic atmosphere. The SEM images of SC and SD were also used to determine the adsorbent size using the ImageJ software.

2.4.4 Particle surface area and pore diameter. The Brunauer–Emmett–Teller (BET) analysis method was used to determine the specific surface area and pore diameter of FNP. It is based on the physical adsorption of gas molecules onto the surface of a solid and provides essential information about the material's surface properties. For this, the FNP was first degassed under nitrogen gas flow to remove contaminants (moisture, adsorbed gases). Then, the particles were analyzed using Quantachrome instruments under nitrogen gas for 12.0 h at an outgas temperature of 300 °C, pressure tolerance of 1.000/1.000 (ads/des), equilibrium time of 30/30 s (ads/des), and equilibrium timeout of 360/360 s (ads/des). The FNP surface area and pore diameter were calculated based on the BET equations employed in the instruments.

2.4.5 pH_{pzc}. To determine pH_{pzc} of the samples, 20 mL of 0.1 M KCl solution was added in a 100 mL Erlenmeyer flask and adjusted the pH to 2, 4, 6, 8, 10, and 12, using 0.1 M NaOH solution or 0.1 M HCl. Then, the samples were subjected to each flask, soaked with continuous shaking for 24 h, and the pH of the solution was assessed again. The differences in the pH before and after soaking (ΔpH), and the initial pH, were used to plot a graph, which determines the sample pH_{pzc} (*i.e.*, the pH where the samples had no net charges).[24]

2.4.6 Chemical interactions. Fourier-transform infrared (FT-IR) spectroscopy was performed to analyze the interactions between MB and the adsorbent materials. FT-IR spectra were obtained using a JASCO FT/IR-6300 spectrometer with a resolution of 1 cm^{-1} over the spectral range of 4000–400 cm^{-1}. This analysis provided insights into functional group interactions and the adsorption mechanism.

2.5 *In silico* molecular docking

To comprehensively investigate the molecular interactions between fibroin and MB, an *in silico* molecular docking approach was employed following standard computational protocols. Initially, the MB ligand underwent energy minimization and structural refinement before being converted into the .pdbqt format. The MMFF94x force field was applied for small-molecule geometry optimization, ensuring appropriate bond lengths, angles, and torsional energies, thereby stabilizing the ligand conformation. The fibroin protein structure was retrieved from the Protein Data Bank (PDB), which was 3UA0,[25] followed by the removal of water molecules, addition of polar hydrogen atoms, and assignment of Kollman charges, after which it was also saved in .pdbqt format. Subsequently, the binding site was identified to ensure that the docking region encompassed both the ligand and the key amino acid residues involved in the interaction. The binding positions and interaction types, including hydrogen bonding, van der Waals forces, and π–π interactions, were examined to assess the complex's affinity and stability. Molecular docking was then executed to estimate the binding affinity and compute the binding free energy (ΔG_dock or docking score (DS)). DS represents the predicted binding free energy, where values below −4 kcal mol^{-1} indicate strong binding affinity. The most favorable configurations, characterized by the lowest DS and an acceptable conformational root-mean-square deviation (RMSD < 2.0 Å), were selected for further structural and energetic analysis.

2.6 Molecular dynamics simulation

To in-depth investigate the interactions between MB and fibroin, especially in the aqueous environment (*i.e.*, fibroin and MB are surrounded by the water molecules), as well as the complex structural stability, molecular dynamics (MD) simulation was employed. To this end, MD simulation was conducted using GROMACS software with an appropriate force field for the protein-ligand system. The initial structures of the protein (PDB ID: 3UA0) and MB were prepared and positioned based on the docking results (Section 2.5). The system was solvated in a simulation box using the TIP3P water model and neutralized with Na^+/Cl^- ions. Following energy minimization and equilibration steps (NVT and NPT ensembles), MD simulation was carried out for 20 ns at 300 K and 1 atm. Analyses performed included RMSD, root mean square fluctuation (RMSF), and ligand-receptor interactions.

2.7 Statistical analysis

All experiments were conducted in triplicate and the quantitative results were presented as mean ± standard deviation. Student's *t*-test and ANOVA statistical tests were employed for samples comparisons, with significant values of $p < 0.05$.

3. Results and discussions

Silk has long been employed in the textile industry, which demonstrates its capacity in adsorbing natural dyes and colorants such as MB.[17] Nevertheless, to the best of our knowledge, as of 03/2025, no in-depth research has investigated the ability of silk, and its main component fibroin, for their ability in the adsorptions of chemicals. Furthermore, little is known about the dye-fibroin molecular interactions. Hence, this work focused on this issue, utilizing SC, SD, and FNP, as three distinct states of fibroin, for the adsorption of a model dye, MB. The research first investigated the adsorbent properties, followed by the adsorption process and kinetics, explained the adsorption mechanisms, and determined the fibroin-MB chemical interactions by *in silico* docking study.

3.1 Characterizations of the adsorbents

In this study, three adsorbents were employed, including the SC (raw silk material), the SD (pure fibroin fiber without sericin), and the FNP (microparticles made from fibroin). SC was used as obtained. SD was made from the sericin-removal process of SC. Specifically, 5 g of dried SC produced 3.85 ± 0.11 g of SD, indicating an efficiency of 77.0 ± 2.2%, which is commensurate with the fibroin composition of silk fibers, which includes 25–27% sericin and 70–75% fibroin.[26] The FNP were produced using the solvent exchange technique. Fibroin has an α-helix structure in solution. When exposed to ethanol, it forms additional hydrogen bonding and transforms into an anti-parallel-β sheet structure, resulting in a particulate system.[19] The particle formation efficiency was 72.1 ± 2.3%.

3.1.1 Total nitrogen content. The total nitrogen content of the SC, SD, and FNP was 16.5 ± 0.12%, 17.0 ± 0.03%, and 16.9 ± 0.02%, respectively. Generally, the standard nitrogen content reported for SC and SD is 16.8 ± 0.01% and 17.4 ± 0.11%.[27] Hence, our values were in well agreement with the literature, suggesting the process validity. The slight increase in nitrogen content in SD was consistent with the known composition of silk cocoons, which typically contain sericin and other impurities with lower nitrogen content than pure fibroin protein. Therefore, the observed increase in nitrogen content upon degumming (SD) and subsequent microparticle processing (FNP) is indicative of the effective removal of sericin and other non-protein constituents, resulting in purer fibroin materials.

3.1.2 Size and morphology. Physically, the appearances of the three adsorbents are illustrated in Fig. 1. Accordingly, the size of FNP was 2.45 ± 0.35 μm, with polydispersity index of 0.052 ± 0.003, indicating narrow size distribution.[28] Whereas, SC and SD were mechanically cut to a size of 1 mm. Fig. 1A showcases raw SC in their natural state. The cocoons are composed of fibroin and sericin proteins, with fibroin serving as the structural core and sericin as the protective outer layer. Fig. 1B depicts silk fibers after the removal of sericin through degumming, resulting in fibroin-dominant fibers. These fibers exhibit a soft, fibrous

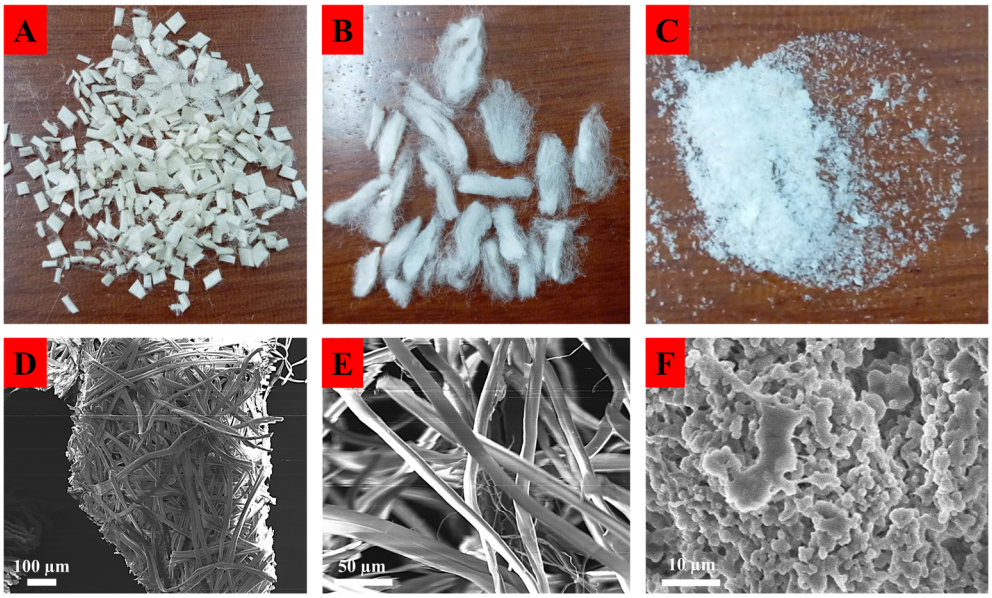

Fig. 1 Physical appearance and SEM images of (A and D) silkworm cocoon (SC), (B and E) sericin-degummed silk strands (SD), and (C and F) fibroin microparticles (FNP).

morphology, with elongated, thread-like structures indicative of their proteinaceous composition. The removal of sericin enhances the biocompatibility and mechanical properties of the fibers, making them suitable for biomedical applications. Fig. 1C illustrates FNP powder, obtained through the process of self-assembly *via* solvent exchange technique. The particles display a fine, powder-like morphology.

Utilizing the SEM techniques, the in-depth structures and morphology of the samples were revealed. Accordingly, the SC composed of different fibers interconnected to each other in the cocoons (Fig. 1D), whereas SD was a long smooth fiber with a diameter of 20.3 ± 1.6 μm and an average length of 1.1 ± 0.2 mm (Fig. 1E). On the other hand, the FNP were spherical with smooth surface (Fig. 1F). The size difference between FNP, SC, and SD results in a difference in surface area, which influences MB's adsorption ability, as later discussed.

3.1.3 pH_{pzc} and chemical interactions. The pH_{pzc} of SC, SD, and FNP are displayed in Fig. 2A. Briefly, SC and SD show an initial rise in ΔpH at lower initial pH values (2–4), followed by a sharp decrease, becoming negative at higher initial pH values. Thus, at normal pH of 7.0 or higher, both SC and SD possessed a negative charge. The FNP exhibit less pronounced pH variation, suggesting a relatively moderate surface charge compared to SC and SD, indicating higher stability and possibly fewer exposed acidic groups due to the transformation from silk I to silk II structures, with more β-sheet content.[19,26] Nevertheless, FNP also had negative charge at pH 6.7 or higher. On the other hand, MB has a pK_a value of 3.8, which corresponds to the demethylation of the dimethylamino group.[29] Nevertheless, MB is a thiazine dye, and its structure includes a permanently charged quaternary nitrogen within the central heterocyclic ring system. This positive charge is not affected by normal acid-base

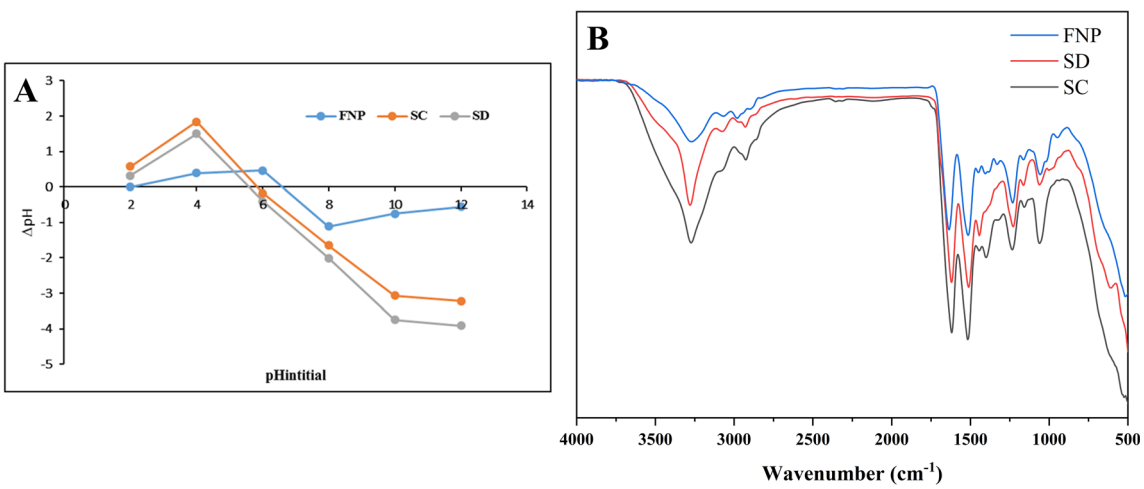

Fig. 2 (A) pH_{pzc} and (B) FT-IR graphs of silkworm cocoon (SC), sericin-degummed silk strands (SD), and fibroin microparticles (FNP).

equilibria. Thus, even at pH > 3.8, specifically at pH > 6.7, the MB side group deprotonates, but the core structure remains positively charged due to the quaternary nitrogen, making MB a cation in this pH.[30] Thus, at pH 7.0 or higher, MB predominantly exists in its positively charged form, making it highly interacted with fibroin *via* ionic interactions, as discussed in the next sections.

Regarding the FT-IR analyses (Fig. 2B), all three spectra share characteristic bands typical of silk fibroin, including broad peaks at ~3300 cm^{-1}, corresponding to O–H and N–H stretching vibrations (hydrogen bonds); peaks at ~2900–3000 cm^{-1} (C–H stretching); and strong absorptions at ~1630 cm^{-1} (amide I), ~1515 cm^{-1} (amide II), and ~1230 cm^{-1} (amide III), reflecting the presence of protein (peptide bonds) of silk fibroin 19. Notably, SC exhibits relatively broader and slightly lower intensity peaks due to impurities or sericin proteins covering fibroin. SD presents sharper and more defined bands compared to SC, indicating removal of sericin and the resultant exposure of pure fibroin. FNP show spectral characteristics similar to SD, with well-defined amide bands. The sharper and clearer peaks in FNP compared to SC suggest effective microparticles formulation.

3.1.4 Particle surface area and pore diameter. FNP are micron-sized, therefore, the increased specific surface area increases the contact area with MB molecules, making interactions easier. To further investigate the MB adsorption behaviors, the FNP surface areas and pore diameter were determined by BET analysis (Fig. 3). FNP have a particular surface area of 21.894 ± 1.120 $m^2\ g^{-1}$ and an average pore size of 21.911 ± 1.711 Å. The nitrogen adsorption–desorption curve (Fig. 3A) follows a type-IV isotherm, typically associated with mesoporous materials. Detailed analysis shows that FNP have an average of 78.79% mesopores (2–50 nm diameter) and 21.21% macropores (>50 nm diameter) (Fig. 3C). These permit MB to easily permeate into the particles, as the surface area of MB molecules is only 1.32 nm^2.[31] The presence of macropores complements mesopores, offering pathways for rapid diffusion and penetration of MB molecules deep within the particle, facilitating efficient internal diffusion and maximizing the utilization of adsorption site. Moreover, the presence of hysteresis (a clear difference between adsorption and desorption curves) suggests significant pore condensation phenomena, enabling better interaction of MB molecules with pore walls through capillary condensation and multilayer adsorption, potentially improving overall adsorption efficiency. Additionally, the narrow distribution of pore sizes centered in the mesoporous region means most adsorption sites are optimally sized for effective trapping and retaining of MB molecules (Fig. 3B). All of the aforementioned factors enhance the adsorption of MB molecules by FNP, allowing for the easy

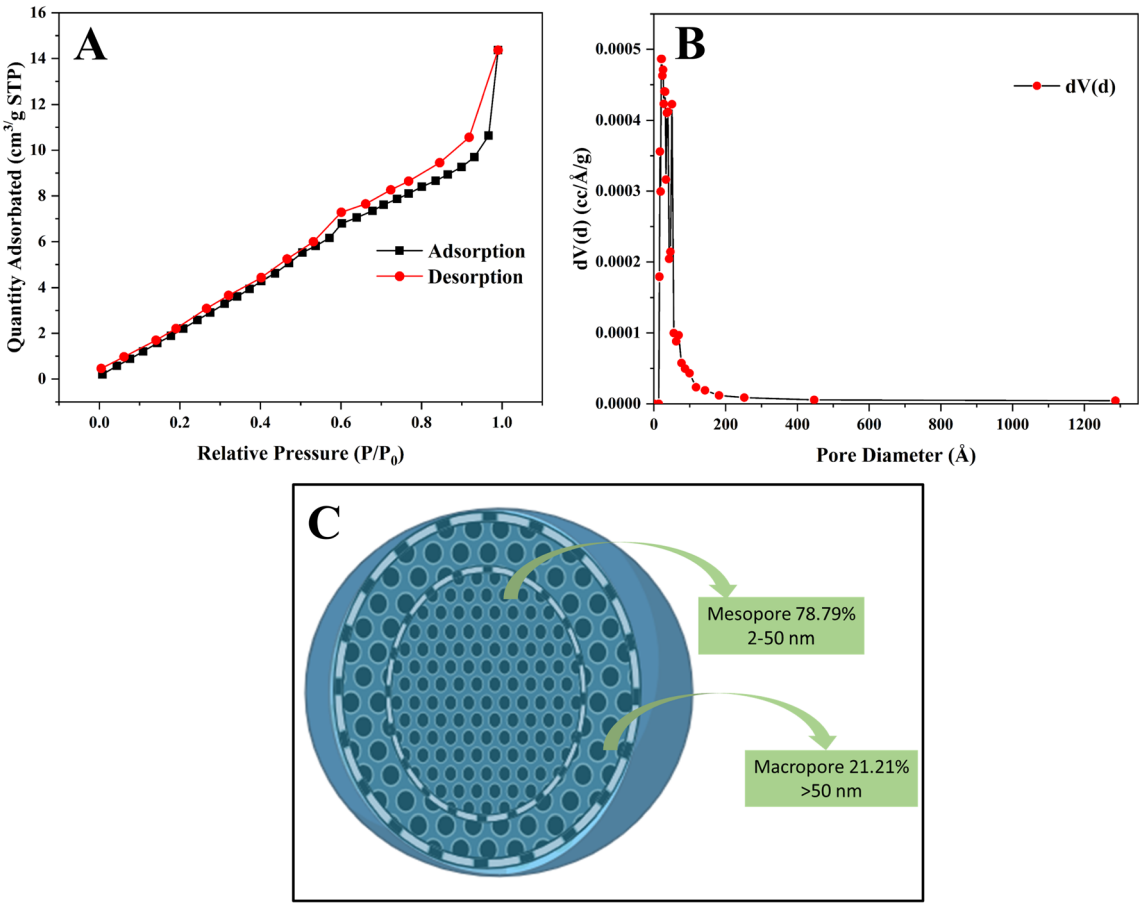

Fig. 3 (A) Surface area analysis, (B) pore diameter, and (C) pore distribution of FNP.

formation of contacts between functional groups in the FNP and MB particle structures.

3.2 MB adsorption investigation

To investigate the adsorption capacity of these three silk-based materials, SC, SD, and FNP, as well as the effects of different adsorption conditions on the process, experiments were conducted at varied initial concentration of MB, mass of SC and SD, mass of FNP, adsorption time, and pH (Fig. 4). Firstly, it is worth to note that the variation in the adsorbent mass was significantly different between SC/SD (0.1, 0.2, 0.4, 0.6, and 0.8 g) and FNP (0.003, 0.006, 0.012, 0.024, and 0.036 g) due to their different adsorption capacity. Thus, there are two graphs (Fig. 4B and C) depicting the mass variation. Accordingly, FNP consistently demonstrated superior results, compared to SC and SD, across all parameters.

The initial MB concentration significantly affected adsorption efficiency. Particularly, efficiency rose as the concentration climbed from 5 μg mL^{-1} to 30 μg mL^{-1}, and plateau at 40 μg mL^{-1}. This trend is typical in adsorption processes, where the saturation of available binding sites limits further adsorption beyond a certain concentration. SC and SD showed better adsorption efficiency than FNP, although their adsorption capacity was less than that of FNP (Fig. 4A). The adsorption capacity of the SC sample rose from 0.37 ± 0.02 mg g^{-1} to 3.8 ± 0.2 mg g^{-1}, the SD sample from 0.38 ± 0.02 to 3.8 ± 0.3 mg g^{-1}, and the FNP from 7.22 ± 0.6 to 122.98 ± 8.4 mg g^{-1}, respectively. This difference highlights the higher affinity of FNP for MB molecules, likely due to its increased surface area and the availability of more binding sites, as later discussed.

According to the adsorbent mass variations, increasing the mass of SC, SD, and FNP significantly decreases the adsorption capacity (Fig. 4B). This suggested that excessive amounts of adsorbents lead to underutilized binding sites, as the available MB molecules are insufficient to saturate all adsorption sites. This rapid decline in with increasing dose reflects the high surface area and porosity of FNP, which allows for rapid saturation of binding sites at lower doses, making it more effective for practical applications where minimal adsorbent usage is desirable. Accordingly, the ideal mass for SC and SD is 0.1 g and 0.006 g for FNP to fully use the material's adsorption capability. It is worth to notice that the FNP had a mass roughly 300 times less than SC and SD, yet their MB adsorption capability was equal, as indicated by the discoloration of the MB solution (Fig. 5). The difference in mass between adsorbent materials SC, SD, and FNP is due to the lower adsorption capacity of SC and SD compared to FNP. On one gram of adsorbent, FNP can adsorb a larger amount of MB than SC and SD, which is related to the material's size and physicochemical properties.

Furthermore, adsorption time is a crucial aspect of the adsorption process since it allows us to develop a kinetic model and calculate the adsorption rate. The adsorption period increased in this experiment, but the adsorption efficiency varied slightly. In the first 15 min of the process, the MB adsorption efficiency of SC, SD, and FNP was 86 ± 1%, 96 ± 2%, and 86 ± 1%, respectively, and remained stable throughout the process (Fig. 4D). This demonstrates that the adsorption speeds

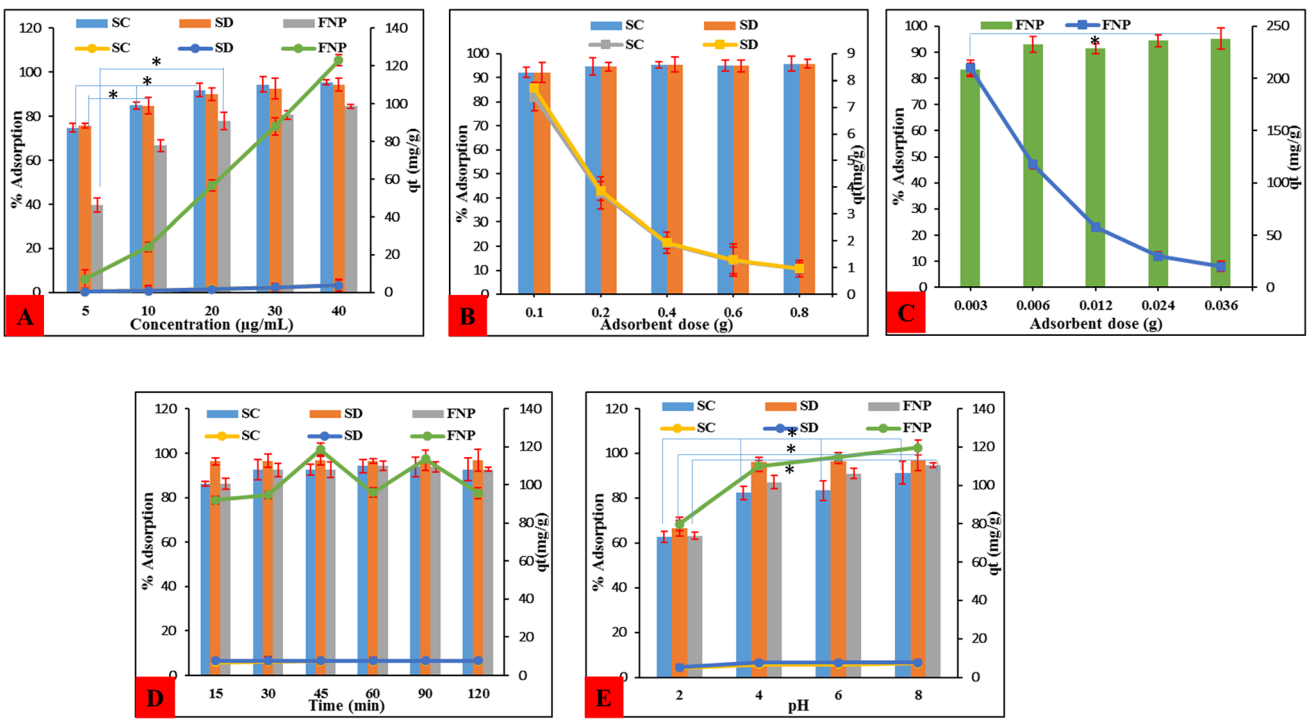

Fig. 4 Experimental investigation of the adsorption capacity of silkworm cocoon (SC), sericin-degummed silk strands (SD), and fibroin microparticles (FNP) on methylene blue (MB), at varied (A) initial concentration of MB, (B) mass of SC, SD, (C) mass of FNP, (D) adsorption time, and (E) pH.

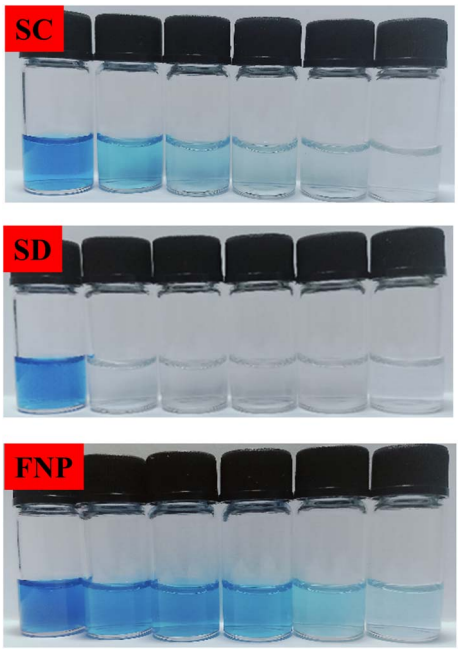

Fig. 5 Differences in mass survey samples between SC, SD, and FNP.

of SC, SD, and FNP were rapid and very effective for MB removal. Furthermore, environmental conditions influence the material's MB adsorption effectiveness, particularly pH, which has a direct impact on the material's charge and hence affects the interaction between the material and MB molecules. When the pH rose from 2 to 8, adsorption efficiency improves (Fig. 4E). This trend is consistent with the electrostatic interactions between the negatively charged surfaces of the adsorbents (proven in the pH_{pzc} graph, Fig. 2) and the cationic MB molecules (discussed in Section 3.1, pH_{pzc}). Notably, FNP exhibits a more pronounced increase in adsorption capacity as pH rises, reaching approximately 120 mg g^{-1} at pH 8, which suggests that the surface chemistry of FNP is more favorable for MB adsorption under alkaline conditions, further contributing to its superior performance compared to SC and SD.

Overall, the results demonstrate that FNP consistently outperforms SC and SD across all tested parameters, with its higher surface area, greater porosity, and faster adsorption kinetics making it the most effective adsorbent for MB. The improved performance of SD compared to SC highlights the importance of removing sericin to enhance the accessibility of fibroin's adsorption sites, further supporting the potential of silk-based materials for MB adsorption.

Notably, in terms of the FNP regeneration/reusability, the MB adsorption efficiency decreased significantly from nearly 100% in the first cycle to 72.94 ± 3.10% in the second cycle, and only 54.31 ± 3.32% in the third cycle. This was possibly due to the fact that MB interacted with fibroin *via* both weak hydrogen bonding and moderate/strong ionic interactions (discussed in the next sections). Thus, some MB molecules was strongly bound to the fibroin structure and was not completely desorbed. Consequently, the adsorption efficiency of the latter cycles was reduced. Further investigations are necessary to confirm this phenomenon.

3.3 Adsorption isotherms and kinetics

When fitting the MB adsorption processes in various kinetics and isothermal models (Fig. S1† and Table 2), the Langmuir and Freundlich adsorption equilibrium models showed coefficients R^2 of >0.9; however, their constants are not appropriate. Langmuir's slope coefficient is less than zero, which contradicts the model premise. The Freundlich model has a coefficient of $n < 1$ (0.14, 0.29, and 0.30 for SC, SD, and FNP, respectively), although the model theory requires $n > 1$.[32] As a result, the Langmuir and Freundlich models are incompatible with the three adsorption processes of SC, SD, and FNP. This fact could be due to (1) heterogeneity of adsorption sites (*i.e.*, the FNP possessed both mesopores (2–50 nm diameter) and macropores (>50 nm diameter), which causes heterogeneity), (2) multi-layer adsorption (Langmuir assumes monolayer adsorption on homogeneous surfaces, while Freundlich typically describes heterogeneous monolayers), and (3) adsorbate–adsorbate interactions (*i.e.*, MB could interact with other MB molecules, leading to the unfitted data). Moreover, as later discussed in the D–R model and *in silico* docking study, MB interacts with fibroin *via* favorable molecular interactions, leading to the chemisorption process.

The D–R model is used to calculate the interactions between materials and MB. The adsorption energies computed by the D–R model for SC, SD, and FNP were 408.25 kJ mol^{-1}, 707.11 kJ mol^{-1}, and 276.26 kJ mol^{-1}, respectively. All these values were far larger than 8 kJ mol^{-1}, showing that the adsorption process was chemisorption.[33] Furthermore, the first-order kinetic model and the second-order kinetic model were used to assess the adsorption rate, which revealed that all three materials' adsorption processes were compatible with the second-order kinetic model. The second-order equation had an R^2 value greater than 0.9, and the adsorption capacity estimated using second-order kinetics was comparable to the experimental capacity. Furthermore, the slope of the equation was quite tiny, suggesting that the material's adsorption rate was extremely high. Conclusively, the MB adsorption process on SC, SD, and FNP were chemisorption and followed the second-order kinetics.

3.4 MB adsorption mechanisms

According to the D–R isotherm model (Section 3.3), the fibroin-MB adsorption process was chemical in nature, with chemical bonds forming between MB and fibroin. Hence, to further investigate this phenomenon, FT-IR spectra of the FNP prior and after MB adsorption (FNP-MB) were analyzed (Fig. 6). The FT-IR spectrum indicated that, beyond the characteristic peaks of FNP, additional signals appeared in the FNP-MB spectrum, confirming interactions with MB. The broad band at ~3330 cm^{-1} in FNP (–OH) overlapped with the –NH stretching of MB, with increased intensity suggesting the formation of new hydrogen bonds.[34] Peaks at 1646 cm^{-1}, 1526 cm^{-1}, and 1229 cm^{-1}, corresponding to amide I, amide II, and amide III of

Table 2 Adsorption equilibrium and adsorption isotherms/kinetics models

Models	SC	SD	FNP
Langmuir isotherm	$y = -5.9046x + 10.6220$ $R^2 = 0.9229$	$y = -2.2275x + 5.5785$ $R^2 = 0.9258$	$y = -0.0811x + 0.5187$ $R^2 = 0.5649$
Freundlich isotherm	$y = 6.9963x - 1.1700$ $R^2 = 0.9455$	$y = 3.4530x - 0.7112$ $R^2 = 0.9871$	$y = 3.3769x - 0.5557$ $R^2 = 0.9031$
D–R isotherm	$y = -3.10^{-6}x + 4.5608$ $R^2 = 0.9302$ $E = 408.25$ kJ mol^{-1}	$y = -10^{-6}x + 2.3716$ $R^2 = 0.9707$ $E = 707.11$ kJ mol^{-1}	$y = -7.10^{-6}x + 5.7167$ $R^2 = 0.9515$ $E = 276.26$ kJ mol^{-1}
Pseudo-first-order kinetics	$y = -0.0009x + 2.4390$ $R^2 = 0.0007$ $K_1 = 0.0009$	$y = -0.0154x - 0.7396$ $R^2 = 0.2363$ $K_1 = 0.0154$	$y = -0.0281x - 1.6120$ $R^2 = 0.357$ $K_1 = 0.0281$
Pseudo-second-order kinetics	$y = 0.1333x + 0.0703$ $R^2 = 0.9997$ $K_2 = 0.25$	$y = 0.1290x + 0.0141$ $R^2 = 1$ $K_2 = 1.18$	$y = 0.0100x - 0.0112$ $R^2 = 0.9748$ $K_2 = 0.009$

FNP, also intensified significantly after MB adsorption.[19] This enhancement is attributed to the resonance effect from the C=N$^+$ vibration of MB's dimethylamino group and the formation of hydrogen bonds between MB and the fibroin amide groups.[34] The peak at 1447 cm^{-1}, attributed to the C–S bond of MB, appeared distinctly in the FT-IR spectrum of FNP-MB, indicating an interaction between the sulfur atom (S$^+$) of MB and the oxygen atom (–OH group) in the fibroin structure.[17] This suggests an electrostatic/ionic or polar interaction, as MB can exist as a cation in solution due to electron loss in its C–S–C heterocycle. Additionally, the nitrogen atom (–N–CH$_3$) in MB may form a covalent bond with oxygen atoms in fibroin amino acid residues, driven by high adsorption energy. The C–N bond is shown by the peak intensity at 1332 cm^{-1}, which rises as MB is adsorbed, confirming the interaction of MB with FNP. Hydrophobic interactions between MB's alkyl chains and fibroin also contribute to the overall binding. Conclusively, the FT-IR spectrum showed that the interactions between MB and FNP formed favorable molecular interactions. A summary of these interactions is presented in Fig. 7.

3.5 *In silico* molecular docking

To specifically point out where the interactions take place between MB and fibroin, the *in silico* docking study was conducted (Fig. 8). Generally, fibroin molecule has two distinct polypeptide chains, the heavy chain and the light chain,

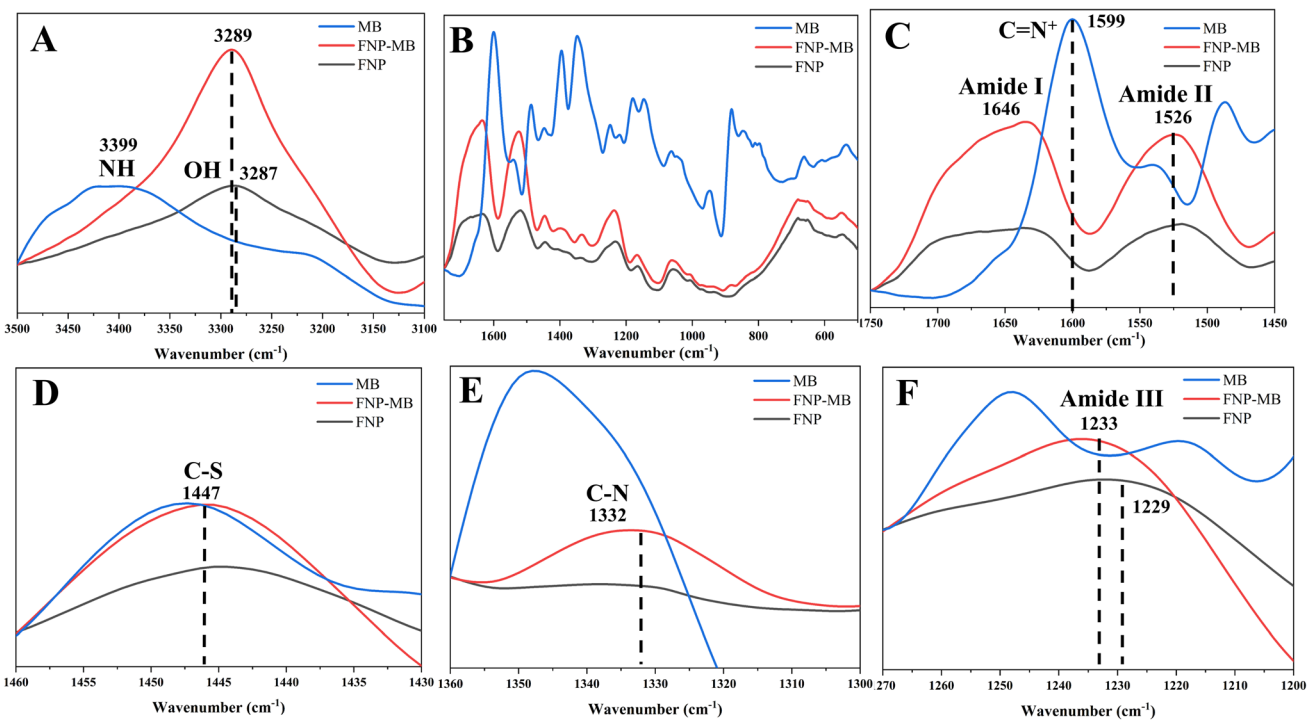

Fig. 6 FT-IR spectrum of the pure MB, FNP before adsorption, and FNP after MB adsorption (FNP-MB), at fibroin characteristic peaks of (A) 3500–3100 cm^{-1}, (B) 1650–650 cm^{-1}, (C) 1750–1450 cm^{-1}, (D) 1460–1430 cm^{-1}, (E) 1360–1300 cm^{-1}, and (F) 1270–1200 cm^{-1}.

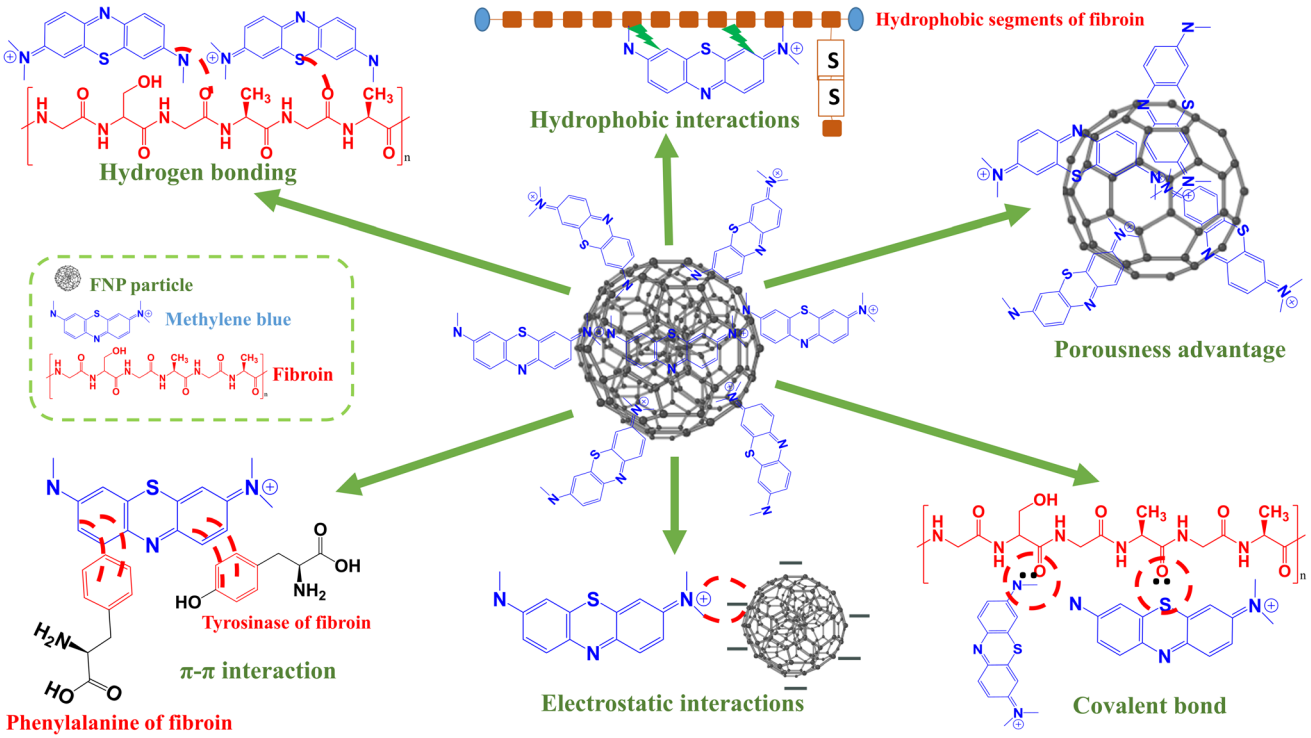

Fig. 7 MB adsorption mechanisms of FNP.

interconnected to each other by a disulfide bond.[26] The docking results revealed that MB had favorable interactions with the heavy chain of fibroin (Table 3). Specifically, MB exhibited a hydrogen bonding with Lys62 (NZ) at a distance of 3.34 Å, with a binding energy of −0.2 kcal mol^{-1}. Most hydrogen bonding has an average binding energy of 1–5 kcal mol^{-1}. However, in some cases, especially in natural-based systems such as fibroin, this bonding can be transient or geometry-dependent, thus reducing its binding energy to 0.5 kcal mol^{-1} or less.[35] In this case, the hydrogen bonding is considered as weak bonding. Additionally, two ionic interactions were observed with Glu94 (OE1 and OE2) at distances of 3.85 Å and 3.51 Å, respectively, with corresponding binding energies of −0.8 kcal mol^{-1} and −1.9 kcal mol^{-1}, indicating favorable moderate-to-strong interactions. The overall DS

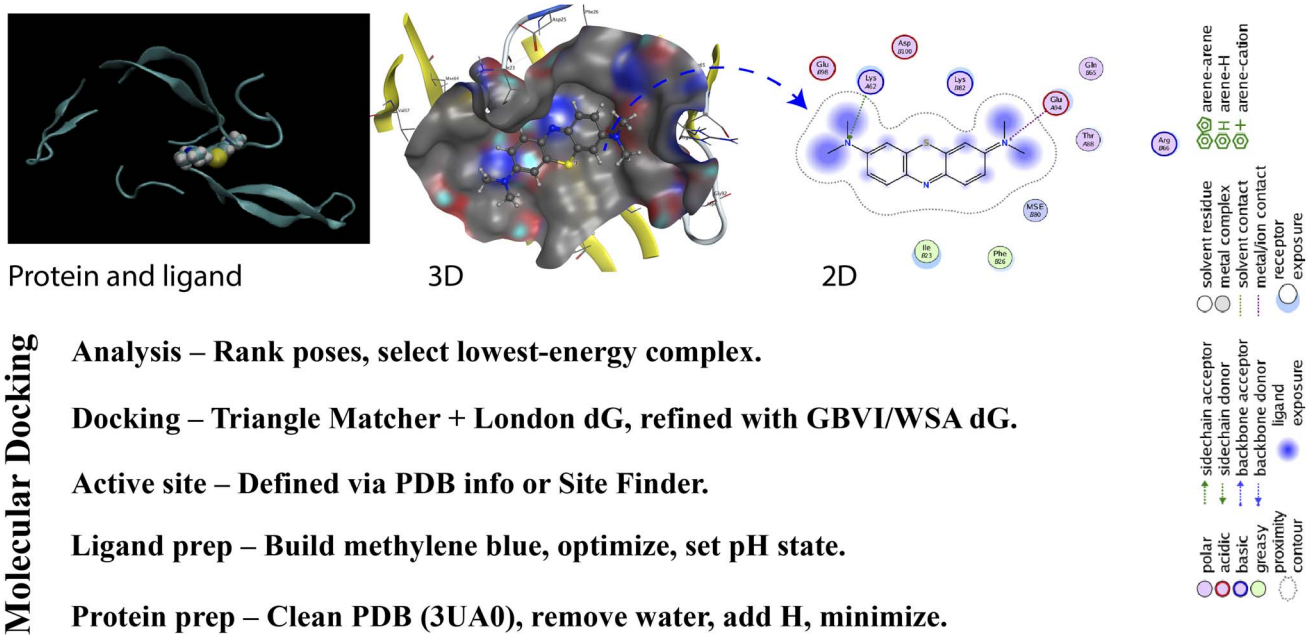

Fig. 8 *In silico* docking study of MB and fibroin molecular interactions.

Table 3 Docking parameters and interactions between MB and fibroin. DS: docking score; RMSD: root mean square deviation; *E*_conf: conformational energy; *E*_place: energy of initial ligand placement; *E*_score1: initial scoring energy; *E*_refine: energy after ligand-receptor refinement step; *E*_score2: final docking scoring energy after refinement. A chain: heavy chain of fibroin

DS (kcal mol^{-1})	RMSD (Å)	*E*_conf	*E*_place	*E*_score1	*E*_refine	*E*_score2
−4.883	1.370	7.296	−28.864	−7.603	−16.606	−4.883

Fibroin amino acid	MB atom	Interaction	Distance (Å)	Energy (kcal mol^{-1})
Lys62 (NZ)-A chain	Nitrogen (position 5)	H-bond acceptor	3.34	−0.2 (weak)
Glu94 (OE1)-A chain	Nitrogen (position 24)	Ionic	3.85	−0.8 (moderate)
Glu94 (OE2)-A chain	Nitrogen (position 24)	Ionic	3.51	−1.9 (strong)

was −4.883 kcal mol^{-1}, indicating a stable interaction between MB and fibroin.[36] Furthermore, the RMSD value (1.370 Å) reflected the agreement between the predicted and experimental structures. The binding energy values were also notable, with *E*_place = −28.864 kcal mol^{-1}, *E*_score1 = −7.603 kcal mol^{-1}, and *E*_refine = −16.606 kcal mol^{-1}, confirming the stability of the formed complex.

Since ionic interactions were the main forces binding MB and fibroin, the MB adsorption process was re-confirmed to be chemisorption, as previously discussed. Previous study has pointed out that MB and fibroin could interact *via* the S atoms of MB and N in lysine and O in tyrosine residues of fibroin.[17] However, these hypothetical claims appeared to be not in agreement with the docking study, which revealed different interactions. These findings highlight the potential of fibroin as an effective adsorbent for charged small molecules, particularly compounds like MB. Compared to previous studies, the interactions observed in this study align with the biochemical properties of fibroin, a protein polymer capable of forming favorable molecular interactions with charged molecules due to the presence of functional groups such as glycine, lysine, and glutamate.[37–41]

3.6 Molecular dynamics simulation

To further investigate the MB and fibroin interactions in the present of water molecules, MD simulation was conducted (Fig. 9). Accordingly, the fibroin-MB complex stability was determined through the RMSD index. Throughout the 20 ns simulation, the RMSD fluctuated between 0.25 and 1.75 nm, stabilizing notably after approximately 6 ns. Firstly, at around 0–2 ns, the RMSD value starts around ~0.25–0.5 nm, indicating the fibroin-MB complex initially remains relatively stable. However, the RMSD exhibits significant fluctuations and peaks around ~1.75 nm near the 5 ns mark, suggesting structural

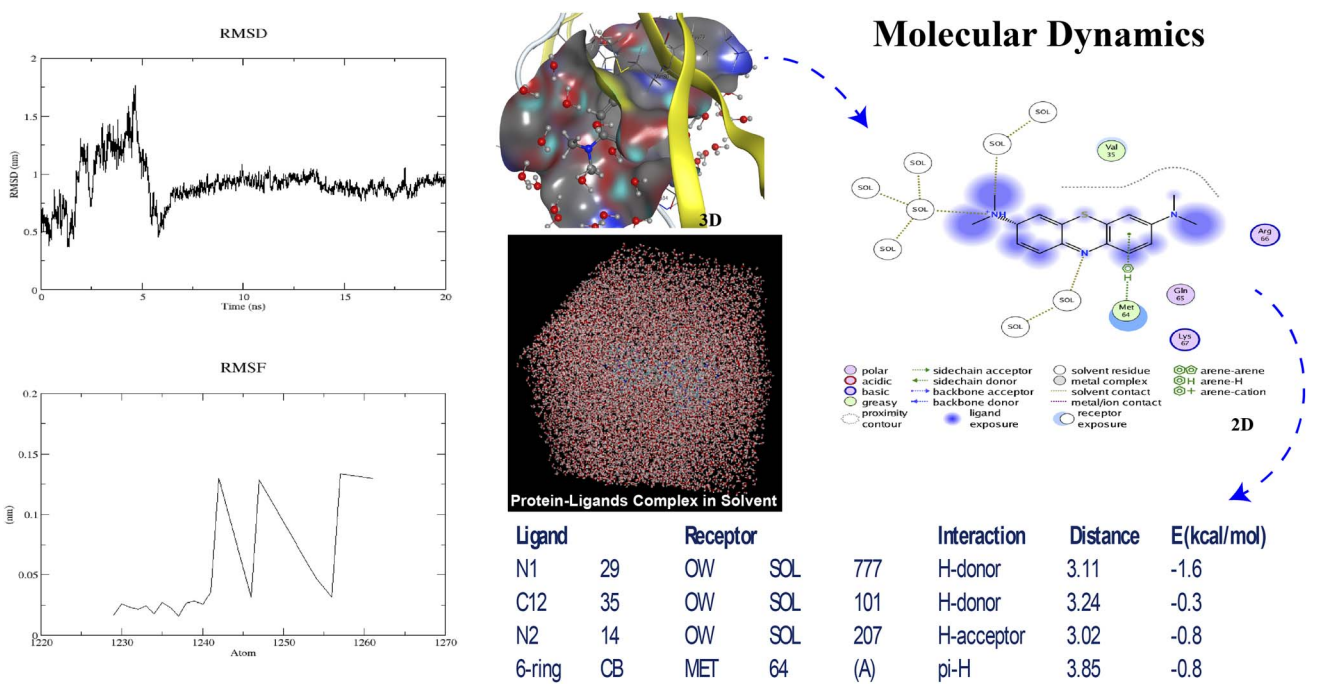

Fig. 9 Molecular dynamics simulation results of MB and fibroin interactions, with RMSD and RMSF plots, the complex structure in water, 3D and 2D representations of molecular interactions, and a table summarizing key ligand-receptor interactions.

rearrangements or conformational adjustments as the complex accommodates or optimizes the ligand binding mode. Finally, after that, in the equilibrium phase, the RMSD sharply decreases and stabilizes around approximately 1.0 nm. This stabilization indicates the complex reaches equilibrium and maintains structural integrity without substantial deviations from the average structure. Conclusively, the fibroin-MB complex becomes structurally stable after 6 ns of simulation time, and a stable RMSD around ~1.0 nm suggests the complex is adequately equilibrated for further structural or energetic analysis.[42]

Moreover, the RMSF analysis reflects atomic fluctuations within specific residues or regions of the protein in the fibroin-MB complex. Specifically, at low RMSF region (atoms ~1230–1240), low fluctuations (~0.02–0.05 nm) were observed, indicative of rigid or constrained atoms, corresponding to stable and tightly bound structural elements such as anti-parallel β-sheet structure of fibroin, and residues potentially involved directly in ligand binding or maintaining protein structure integrity.[43] On the other hand, at higher RMSF peaks (atoms ~1240–1265), clearer fluctuations appear (~0.02–0.15 nm). This indicates higher flexibility, which is characteristic of loop regions, terminal residues, or amino acids less involved directly in structural stability or ligand binding.[44] Overall, the fluctuations below 0.15 nm suggest no significant structural changes in the fibroin at the interaction site. This stability is essential to maintaining the integrity of binding between MB and the fibroin active regions.[45,46] Conclusively, the fibroin-MB complex is stable in the aqueous environment.

Interestingly, the analysis of 3D visualizations and the hydrated fibroin-MB complex model indicated that MB is well surrounded/solvated by water molecules in the aqueous environment, increasing the accuracy of simulating real aqueous conditions (Fig. 9, central image). Despite solvation, MB consistently formed three hydrogen bonds with water molecules and fibroin ($E = -1.6$ kcal mol^{-1} (strong), -0.8 kcal mol^{-1} (moderate), and -0.3 (weak) kcal mol^{-1}), along with one π–H interaction between the six-membered aromatic ring of MB and residue Met 64 (A chain), with a distance of 3.85 Å and energy of -0.8 kcal-mol^{-1}, as summarized in the interaction table. These interactions remained stable over time, as shown by the converged RMSD plot (top left) and low local fluctuations in RMSF (bottom left), supporting the formation of a thermodynamically stable complex. Therefore, the directional, energetically favorable interactions between MB and fibroin in the presence of water are fully consistent with docking and FT-IR evidences of chemisorption.

3.7 Comparisons with previous work

To the best of our knowledge, as of 03/2025, no study has been reported on the utilization of FNP for MB adsorption. Hence, we conducted this work to fill in the literature gaps, with a focus on fibroin-MB molecular interactions. Accordingly, a brief summary and comparison between relevant fibroin/silk-based materials for MB adsorption is presented in Table 4. Accordingly, FNP could significantly increase the adsorption efficiency compared to the raw silk and degummed silk. Moreover, the blending of fibroin with hydroxypropyl methylcellulose (HPMC), as in silk fibroin/HPMC microparticles, exhibited the highest sorption capacities (490–512 mg g^{-1}), far surpassing other silk-based adsorbents,[13] which can be attributed to the presence of HPMC that enhances interaction sites or internal porosity for dye adsorption. Additionally, adsorbents with higher S_{BET} values (*i.e.*, high surface area and porosity) demonstrated higher adsorption capacity, in agreement with previous studies.[8,12,14] Similarly, smaller particle sizes typically improve adsorption performance due to higher surface availability. Indeed, the microparticle forms demonstrated significantly better adsorption capacities compared to larger structures such as SC and SD. Interestingly, exceptionally small particles (ultrafine silk fibroin powder, 3.8 μm) still exhibited modest adsorption (20.58 mg g^{-1}), implying that size reduction alone might not be sufficient without adequate surface functionalities or porosity. Notably, between similar materials of SC and SD, our study showed less adsorption capacity compared to previous works,[17] which could be attributed to variations in silk source, degumming methods, processing conditions, and structural integrity post-treatment. Further research could in-depth explore these differences.

When comparing between FNP and other well-established adsorbents, traditional adsorbents like activated carbon, graphene oxide, and carbon nanotubes offer high adsorption capacities, most notably graphene oxide at 951.35 mg g^{-1} and activated carbon at up to 148.8 mg g^{-1} (Table 4). Nevertheless, these inorganic materials also come with significant drawbacks. They often require energy-intensive or chemically aggressive synthesis routes, involve toxic precursors, and pose risks of secondary environmental contamination due to their non-biodegradable nature and potential cytotoxicity.[48,50] In contrast, FNP, with an adsorption capacity of 122.98 mg g^{-1}, offer a unique combination of efficiency, eco-friendliness, and biocompatibility.[26] Silk fibroin is a natural protein-based biopolymer that has been approved by the US Food and Drug Administration (US FDA) as a biomaterial that can be used in numerous biomedical and pharmaceutical applications.[26] Upon degradation, fibroin primarily yields peptides and amino acids, which are non-toxic and biodegradable in aquatic environments.[52] Moreover, FNP moderate surface area (21.894 m^2 g^{-1}) coupled with rich functional groups enables effective chemisorption through chemical bonding, as previously discussed. Additionally, FNP can be further tailored structurally and chemically with minimal environmental impact. Last but not least, when roughly compared the production cost (Table 4), FNP presents a compelling balance between affordability and performance when compared to other widely used adsorbents such as activated carbon. While activated carbon is significantly cheaper due to its large-scale industrial production from low-cost biomass (*i.e.*, coconut shells), its manufacturing process involves high-temperature carbonization and activation, which can raise environmental concerns due to energy demands and potential emission of greenhouse gases. In contrast, FNP are derived from renewable silk waste or agricultural by-products and prepared through relatively benign aqueous processes, making them more environmentally friendly and sustainable,

Table 4 Summary and comparison between relevant fibroin/silk-based materials and other established materials for MB adsorption. PSO: pseudo-second-order kinetics; HPMC: hydroxypropyl methylcellulose; D–R: Dubinin–Radushkevich isotherm

Adsorbent	Average sorption capacity (mg g^{-1})	Size/S_{BET}	Adsorption models	Estimated production cost (USD/g)[a]	Ref.
Silk-based materials					
Ultrafine silk fibroin powder	20.58	Size: 3.8 μm	Langmuir	0.2	47
Silk fibroin/HPMC blended microparticles	490–512	Size: ~10 μm	PSO, Langmuir	0.4	13
Raw silk	137.08	S_{BET}: 58.37 m^2 g^{-1}	PSO, Langmuir	0.05	17
Degummed silk	179.14	S_{BET}: 199.46 m^2 g^{-1}	PSO, Langmuir	0.1	17
Silk cocoon fibers	86.2	N/A	PSO, Langmuir	0.05	15
Silkworm cocoons (SC)	3.8	Size: 1 mm^2	PSO, D–R	0.05	This study
Degummed silk (SD)	3.8	Diameter: 20.3 ± 1.6 μm Length: 1.1 ± 0.2 mm	PSO, D–R	0.1	
Fibroin microparticles (FNP)	122.98	Size: 2.45 ± 0.35 μm S_{BET}: 21.894 m^2 g^{-1}	PSO, D–R	0.2	
Other established materials					
Activated carbon	148.8	S_{BET}: 1771, 2120, and 2490 m^2 g^{-1}	PSO, Langmuir	0.05	48
Chitosan composites	128.67	S_{BET}: 380.22 m^2 g^{-1}	Langmuir	0.2	49
Graphene oxide	951.35	Size: 1.0–1.12 mm S_{BET}: 99.055 m^2 g^{-1}	PSO, D–R	2.0	50
Multi-walled carbon nanotubes	95.30	S_{BET}: 118.9 m^2 g^{-1}	PSO, Langmuir	1.5	51

[a] For lab-scale comparison purpose only. The estimated production costs were approximated based on the commercial prices of the corresponding products and raw materials derived from locally available natural sources. These estimations were further refined by incorporating general assumptions regarding electricity consumption and machinery operation costs associated with the extraction, purification, and formulation processes. The exact production costs might be different than these values.

albeit at a slightly higher production cost. Graphene oxide, although showing the highest adsorption capacity, has the highest production cost (2.0 USD per g). Ultimately, while FNP may not be the cheapest material, they represent a cost-effective and sustainable middle ground, especially suitable for environmentally conscious water treatment.

4. Conclusion

This study successfully formulated FNP with high MB adsorption of 122.98 mg g^{-1}, nearly 40 times higher than the raw unprocessed silk materials; and deeply investigated the molecular chemical interactions between fibroin and MB. Several critical factors influencing adsorption efficacy were identified, including initial MB concentration, adsorbent dosage, contact duration, and solution pH. Interestingly, *in silico* docking studies revealed that MB interacts with fibroin mainly *via* chemical bonding, particularly at the fibroin residues Lys62 and Glu94. Furthermore, molecular dynamics simulations under aqueous conditions demonstrated significant stabilization of the fibroin-MB complex, with MB molecules fully encapsulated by water and strengthened through the formation of three additional hydrogen bonds (binding energies ranging from −0.3 to −1.6 kcal mol^{-1}). The limitation of this study is the absence of real MB-contaminated wastewater samples, as the research primarily focused on elucidating the specific interactions between fibroin and MB without the interference of competing ions or compounds. Future investigations should incorporate real wastewaters to provide a more comprehensive assessment of the adsorption performance. Moreover, thermodynamic investigations were lacking and should be employed in future studies. Conclusively, silk fibroin-based adsorbents demonstrate significant potential for MB adsorption, but performance is greatly dependent upon particle size, specific surface area, functionalization, and structural modification (such as degumming).

Data availability

All data underlying the findings described in their manuscript are fully available without restriction.

Author contributions

Conceptualization: D. T. P., B. T. P. T.; methodology: D. T. P., P. T. M. H., N. B. P., N. Y. N., N. T. V., D. D. K., D. S. R., A. M. P-P., M. Q. N., B. T. P. T.; investigation: D. T. P., P. T. M. H., N. B. P., N. Y. N., N. T. V., D. D. K., D. S. R., A. M. P-P., M. Q. N.; data curation: D. T. P., B. T. P. T.; validation: D. T. P., B. T. P. T.; project administration: D. T. P., B. T. P. T.; resource: B. T. P. T.; writing-original draft: D. T. P., B. T. P. T.; writing-review and editing: D. T. P., P. T. M. H., N. B. P., N. Y. N., N. T. V., D. D. K., D. S. R., A. M. P-P., M. Q. N., B. T. P. T. All authors have read and agreed to the published version of the manuscript.

Conflicts of interest

None to declare.

Acknowledgements

This research is funded by Van Lang University, Vietnam under grant number VLU-2503-DT-KCB-GV-0046. In memory of the late Dr Trinh Trung Tri Dang (Tra Vinh University), whose insightful ideas have significantly inspired and guided this research. The authors thank Can Tho University of Medicine and Pharmacy for supporting this study.

References

1 A. Miclescu and L. Wiklund, Methylene blue, an old drug with new indications?, *Rom. J. Anestha. Intensive Care*, 2014, 35–41.
2 M. Ismail, K. Akhtar, M. I. Khan, T. Kamal, M. A. Khan, A. M. Asiri, J. Seo and S. B. Khan, Pollution, toxicity and carcinogenicity of organic dyes and their catalytic bioremediation, *Curr. Pharm. Des.*, 2019, **25**, 3645–3663, DOI: **10.2174/1381612825666191021142026**.
3 A. K. Sarkar Phyllis, G. Tortora and I. Johnson, Review on methylene blue: its properties, uses, toxicity and photodegradation, *Water*, 2022, **14**, 242, DOI: **10.5040/9781501365072.12105**.
4 S. Muzammal, A. Ahmad, M. Sheraz, J. Kim, S. Ali, M. B. Hanif, I. Hussain, S. Pandiaraj, A. Alodhayb, M. S. Javed, H. A. Z. Al-bonsrulah and M. Motola, Polymer-supported nanomaterials for photodegradation: unraveling the methylene blue menace, *Energy Convers. Manage.: X*, 2024, **22**, 100547, DOI: **10.1016/j.ecmx.2024.100547**.
5 A. E. Gahrouei, S. Vakili, A. Zandifar and S. Pourebrahimi, From wastewater to clean water: recent advances on the removal of metronidazole, ciprofloxacin, and sulfamethoxazole antibiotics from water through adsorption and advanced oxidation processes (AOPs), *Environ. Res.*, 2024, **252**, 119029, DOI: **10.1016/j.envres.2024.119029**.
6 S. Pourebrahimi and M. Pirooz, Functionalized covalent triazine frameworks as promising platforms for environmental remediation: a review, *Clean. Chem. Eng.*, 2022, **2**, 100012, DOI: **10.1016/j.clce.2022.100012**.
7 A. E. Gahrouei, A. Rezapour, M. Pirooz and S. Pourebrahimi, From classic to cutting-edge solutions: a comprehensive review of materials and methods for heavy metal removal from water environments, *Desalin. Water Treat.*, 2024, **319**, 100446, DOI: **10.1016/j.dwt.2024.100446**.
8 B. H. Hameed, A. T. M. Din and A. L. Ahmad, Adsorption of methylene blue onto bamboo-based activated carbon: kinetics and equilibrium studies, *J. Hazard. Mater.*, 2007, **141**, 819–825, DOI: **10.1016/j.jhazmat.2006.07.049**.
9 M. Rahimihaghighi, M. Gigli and V. C. A. Ficca, Lignin-derived sustainable nano-platforms a multifunctional solution for an efficient dye removal, *ChemSusChem*, 2024, **17**, e202400841.
10 A. Baburaj and S. Das, Dye fed silkworms to produce naturally coloured silk cocoons, *J. Nat. Fibers*, 2022, **19**, 5651–5662, DOI: **10.1080/15440478.2021.1889430**.

11 H. P. Zhao, X. Q. Feng, S. W. Yu, W. Z. Cui and F. Z. Zou, Mechanical properties of silkworm cocoons, *Polymer*, 2005, **46**, 9192–9201, DOI: 10.1016/j.polymer.2005.07.004.

12 L. J. Martis, N. Parushuram and Y. Sangappa, Preparation, characterization, and methylene blue dye adsorption study of silk fibroin–graphene oxide nanocomposites, *Environ. Sci.: Adv.*, 2022, **1**, 285–296, DOI: 10.1039/D1VA00047K.

13 N. Parushuram, R. Ranjana, B. Narayana, M. Mahendra and Y. Sangappa, Facile fabrication of silk fibroin microparticles: their characterization and potential adsorption study, *J. Dispersion Sci. Technol.*, 2021, 1513.

14 S. Rastogi and B. Kandasubramanian, Progressive trends in heavy metal ions and dyes adsorption using silk fibroin composites, *Environ. Sci. Pollut. Res. Int.*, 2020, **27**, 210–237, DOI: 10.1007/s11356-019-07280-7.

15 M. Yavari and N. Salman Tabrizi, Adsorption of methylene blue from aqueous solutions by silk cocoon, *Int. J. Eng.*, 2016, **29**, 1191–1197.

16 D. T. Pham, D. X. T. Nguyen, R. Lieu, Q. C. Huynh, N. Y. Nguyen, T. T. B. Quyen and V. D. Tran, Silk nanoparticles for the protection and delivery of guava leaf (*Psidium guajava* L.) extract for cosmetic industry, a new approach for an old herb, *Drug Deliv.*, 2023, **30**, 2168793, DOI: 10.1080/10717544.2023.2168793.

17 S. Gupta and B. Kandasubramanian, Silk adsorbent for green and efficient removal of methylene blue from wastewater, *Environ. Sci. Pollut. Res.*, 2024, DOI: 10.1007/s11356-024-33226-9.

18 N. Y. Nguyen, T. N. P. Nguyen, N. N. Huyen, V. D. Tran, T. T. B. Quyen, H. V. T. Luong and D. T. Pham, Onto the differences in formulating micro-/nanoparticulate drug delivery system from thai silk and vietnamese silk: a critical comparison, *Heliyon*, 2023, **9**, e16966, DOI: 10.1016/j.heliyon.2023.e16966.

19 D. T. Pham, N. Saelim and W. Tiyaboonchai, Crosslinked fibroin nanoparticles using EDC or PEI for drug delivery: physicochemical properties, crystallinity and structure, *J. Mater. Sci.*, 2018, **53**, 14087–14103.

20 D. T. Pham, T. K. Q. Ha, M. Q. Nguyen, V. D. Tran, V. B. Nguyen and T. T. B. Quyen, Silk fibroin nanoparticles as a versatile oral delivery system for drugs of different biopharmaceutics classification system (BCS) classes: a comprehensive comparison, *J. Mater. Res.*, 2022, **37**, 4169–4181, DOI: 10.1557/S43578-022-00782-0.

21 M. Ghaedi, A. G. Nasab and S. Khodadoust, Application of activated carbon as adsorbents for efficient removal of methylene blue: kinetics and equilibrium study, *J. Ind. Eng. Chem.*, 2014, **20**, 2317–2324.

22 N. N. T. Nguyen, D. T. Pham, D. T. Nguyen and T. T. L. Trinh, Bilayer tablets with sustained-release metformin and immediate-release sitagliptin: preparation and *in vitro*/*in vivo* evaluation, *J. Pharm. Invest.*, 2021, **51**, 579–586, DOI: 10.1007/S40005-021-00533-Z.

23 D. T. M. Huynh, V.-H. Tran, M.-N. T. Le, V.-H. Huynh and D. T. Pham, Floating tablets incorporating curcumin solid dispersion as a potential pharmaceutical dosage form for stomach cancer treatment, *J. Appl. Pharm. Sci.*, 2022, **13**, 240–250, DOI: 10.7324/JAPS.2023.114417.

24 Lj. S. Čerović, S. K. Milonjić, M. B. Todorović, M. I. Trtanj, Y. S. Pogozhev, Y. Blagoveschenskii and E. A. Levashov, Point of zero charge of different carbides, *Colloids Surf., A*, 2007, **297**, 1–6.

25 Y.-X. He, N.-N. Zhang, W.-F. Li, N. Jia, B.-Y. Chen, K. Zhou, J. Zhang, Y. Chen and C.-Z. Zhou, N-terminal domain of *Bombyx mori* fibroin mediates the assembly of silk in response to pH decrease, *J. Mol. Biol.*, 2012, **418**, 197–207, DOI: 10.1016/j.jmb.2012.02.040.

26 D. T. Pham and W. Tiyaboonchai, Fibroin nanoparticles: a promising drug delivery system, *Drug Deliv.*, 2020, **27**, 431–448, DOI: 10.1080/10717544.2020.1736208.

27 T. Ngô and T. Bechtold, Analysis of the fibroin solution state in calcium chloride/water/ethanol for improved understanding of the regeneration process, *Fibres Text. East. Eur.*, 2018, **26**, 43–50, DOI: 10.5604/01.3001.0012.5174.

28 D. T. Pham, N. Saelim and W. Tiyaboonchai, Design of experiments model for the optimization of silk fibroin based nanoparticles, *Int. J. Appl. Pharm.*, 2018, **10**, 195–201, DOI: 10.22159/ijap.2018v10i5.28139.

29 T. K. Sen, Adsorptive removal of dye (methylene blue) organic pollutant from water by pine tree leaf biomass adsorbent, *Processes*, 2023, **11**, 1877, DOI: 10.3390/pr11071877.

30 H. R. Sousa, L. S. Silva, P. A. A. Sousa, R. R. M. Sousa, M. G. Fonseca, J. A. Osajima and E. C. Silva-Filho, Evaluation of methylene blue removal by plasma activated palygorskites, *J. Mater. Res. Technol.*, 2019, **8**, 5432–5442, DOI: 10.1016/j.jmrt.2019.09.011.

31 F. Bergaya, G. Lagaly and M. Vayer, *Cation and Anion Exchange*, Elsevier Ltd, 2nd edn, 2013, DOI: 10.1016/B978-0-08-098259-5.00013-5.

32 A. O. Dada, A. P. Lekan, A. M. Olatunya and O. Dada, Temkin and Dubinin–Radushkevich isotherms studies of equilibrium sorption of Zn 2+ unto phosphoric acid modified rice husk, *IOSR J. Appl. Chem.*, 2012, **3**, 38–45, DOI: 10.9790/5736-0313845.

33 N. Y. Nguyen, H. V. T. Luong, D. T. Pham, T. B. Q. Tran and H. G. Dang, Chitosan-functionalized Fe_3O_4@SiO_2 nanoparticles as a potential drug delivery system, *Chem. Pap.*, 2022, **76**, 4561–4570, DOI: 10.1007/S11696-022-02189-X.

34 O. V. Ovchinnikov, A. V. Evtukhova, T. S. Kondratenko, M. S. Smirnov, V. Y. Khokhlov and O. V. Erina, Manifestation of intermolecular interactions in FTIR spectra of methylene blue molecules, *Vib. Spectrosc.*, 2016, **86**, 181–189, DOI: 10.1016/j.vibspec.2016.06.016.

35 A. R. Fersht, J. P. Shi, J. Knill-Jones, D. M. Lowe, A. J. Wilkinson, D. M. Blow, P. Brick, P. Carter, M. M. Waye and G. Winter, Hydrogen bonding and biological specificity analysed by protein engineering, *Nature*, 1985, **314**, 235–238, DOI: 10.1038/314235a0.

36 H. Nassar, W. Sippl, R. A. Dahab and M. Taha, Molecular docking, molecular dynamics simulations and *in vitro* screening reveal cefixime and ceftriaxone as GSK3β

covalent inhibitors, *RSC Adv.*, 2023, **13**, 11278–11290, DOI: 10.1039/D3RA01145C.

37 P. Chomchalao, N. Saelim and W. Tiyaboonchai, Preparation and characterization of amphotericin B-loaded silk fibroin nanoparticles-*in situ* hydrogel composites for topical ophthalmic application, *J. Mater. Sci.*, 2022, **57**, 12522–12539, DOI: 10.1007/S10853-022-07413-3.

38 P. Chomchalao, N. Saelim, S. Lamlertthon, P. Sisopa and W. Tiyaboonchai, Mucoadhesive hybrid system of silk fibroin nanoparticles and thermosensitive *in situ* hydrogel for amphotericin B delivery: a potential option for fungal keratitis treatment, *Polymers*, 2024, **16**, 148, DOI: 10.3390/polym16010148.

39 P. Chomchalao, P. Nimtrakul, D. T. Pham and W. Tiyaboonchai, Development of amphotericin B-loaded fibroin nanoparticles: a novel approach for topical ocular application, *J. Mater. Sci.*, 2020, **55**, 5268–5279, DOI: 10.1007/S10853-020-04350-X.

40 D. T. Pham, N. Saelim and W. Tiyaboonchai, Alpha mangostin loaded crosslinked silk fibroin-based nanoparticles for cancer chemotherapy, *Colloids Surf., B*, 2019, **181**, 705–713, DOI: 10.1016/j.colsurfb.2019.06.011.

41 D. T. Pham, N. Saelim and W. Tiyaboonchai, Paclitaxel loaded EDC-crosslinked fibroin nanoparticles: a potential approach for colon cancer treatment, *Drug Delivery Transl. Res.*, 2019, **10**, 413–424, DOI: 10.1007/s13346-019-00682-7.

42 N. A. Gonzalez, B. A. Li and M. E. McCully, The stability and dynamics of computationally designed proteins, *Protein Eng., Des. Sel*, 2022, **35**, gzac001, DOI: 10.1093/protein/gzac001.

43 D. Zhang and R. Lazim, Application of conventional molecular dynamics simulation in evaluating the stability of apomyoglobin in urea solution, *Sci. Rep.*, 2017, **7**, 44651, DOI: 10.1038/srep44651.

44 S. Sinehbaghizadeh, A. Saptoro, S. Amjad-Iranagh and A. H. Mohammadi, Molecular dynamics simulations of the stability and dissociation of structure-H clathrate hydrates in the presence of different amino acids, gas species, and sH hydrate formers, *Energy Fuels*, 2023, **37**, 10550–10566, DOI: 10.1021/acs.energyfuels.3c01312.

45 D. T. Pham, T. T. D. Le, N. Y. Nguyen, C. K. T. Duc, N. T. Tuan, H. V. T. Luong, Q. T. B. Tran, M. Q. Nguyen and B. T. P. Thuy, PEGylated Silk fibroin nanoparticles for oral antibiotic delivery: insights into drug-carrier interactions and process greenness, *ACS Omega*, 2025, **10**, 11627–11641, DOI: 10.1021/acsomega.5c01089.

46 A. Patan, V. Aanandhi and P. Gopinath, Molecular dynamics simulation approach of hybrid chalcone–thiazole complex derivatives for DNA gyrase B inhibition: lead generation, *RSC Adv.*, 2023, **13**, 24291–24308, DOI: 10.1039/D3RA00732D.

47 S. Xiao, Z. Wang, H. Ma, H. Yang and W. Xu, Effective removal of dyes from aqueous solution using ultrafine silk fibroin powder, *Adv. Powder Technol.*, 2014, **25**, 574–581, DOI: 10.1016/j.apt.2013.09.007.

48 H. M. El-Bery, M. Saleh, R. A. El-Gendy, M. R. Saleh and S. M. Thabet, High adsorption capacity of phenol and methylene blue using activated carbon derived from lignocellulosic agriculture wastes, *Sci. Rep.*, 2022, **12**, 5499, DOI: 10.1038/s41598-022-09475-4.

49 E. Igberase and I. G. Mkhize, Efficient adsorption of methylene blue (MB) by an eco-friendly chitosan derivative adsorbent: an RSM and ANN modeling study, *Desalin. Water Treat.*, 2025, **321**, 100943, DOI: 10.1016/j.dwt.2024.100943.

50 H. V. T. Luong, T. P. Le, T. L. T. Le, H. G. Dang and T. B. Q. Tran, A graphene oxide based composite granule for methylene blue separation from aqueous solution: adsorption, kinetics and thermodynamic studies, *Heliyon*, 2024, **10**, e28648, DOI: 10.1016/j.heliyon.2024.e28648.

51 V. Selen, Ö. Güler, D. Özer and E. Evin, Synthesized multi-walled carbon nanotubes as a potential adsorbent for the removal of methylene blue dye: kinetics, isotherms, and thermodynamics, *Desalin. Water Treat.*, 2016, **57**, 8826–8838, DOI: 10.1080/19443994.2015.1025851.

52 M. A. Koperska, D. Pawcenis, J. M. Milczarek, A. Blachecki, T. Łojewski and J. Łojewska, Fibroin degradation – critical evaluation of conventional analytical methods, *Polym. Degrad. Stab.*, 2015, **120**, 357–367, DOI: 10.1016/J.POLYMDEGRADSTAB.2015.07.006.